Altered terminal Schwann cell morphology precedes denervation in SOD1 mice

Dario I. Carrasco, *Emory University*
Kevin L. Seburn, *Jackson Laboratory*
Martin Pinter, *Emory University*

Journal Title: Experimental Neurology
Volume: Volume 275
Publisher: Elsevier | 2016-01-01, Pages 172-181
Type of Work: Article | Post-print: After Peer Review
Publisher DOI: 10.1016/j.expneurol.2015.09.014
Permanent URL: https://pid.emory.edu/ark:/25593/rw6h7

Final published version: http://dx.doi.org/10.1016/j.expneurol.2015.09.014

HHS Public Access

Author manuscript

Exp Neurol. Author manuscript; available in PMC 2017 January 01.

Published in final edited form as:

Exp Neurol. 2016 January ; 275(0 1): 172–181. doi:10.1016/j.expneurol.2015.09.014.

Altered terminal Schwann cell morphology precedes denervation in SOD1 mice

Dario I. Carrasco[1], **Kevin L. Seburn**[2], and **Martin J. Pinter**[1]

[1]Department of Physiology, Emory University, Atlanta, GA, USA

[2]The Jackson Laboratory, Bar Harbor, ME, USA

Abstract

In mice that express SOD1 mutations found in human motor neuron disease, degeneration begins in the periphery for reasons that remain unknown. At the neuromuscular junction (NMJ), terminal Schwann cells (TSCs) have an intimate relationship with motor terminals and are believed to help maintain the integrity of the motor terminal. Recent evidence indicates that TSCs in some SOD1 mice exhibit abnormal functional properties, but other aspects of possible TSC involvement remain unknown. In this study, an analysis of TSC morphology and number was performed in relation to NMJ innervation status in mice which express the G93A SOD1 mutation. At P30, all NMJs of the fast medial gastrocnemius (MG) muscle were fully innervated by a single motor axon but 50% of NMJs lacked TSC cell bodies and were instead covered by the processes of Schwann cells with cell bodies located on the preterminal axons. NMJs in P30 slow soleus muscles were also fully innervated by single motor axons and only 5% of NMJs lacked a TSC cell body. At P60, about 25% of MG NMJs were denervated and lacked labeling for TSCs while about 60% of innervated NMJs lacked TSC cell bodies. In contrast, 96% of P60 soleus NMJs were innervated while 9% of innervated NMJs lacked TSC cell bodies. The pattern of TSC abnormalities found at P30 thus correlates with the pattern of denervation found at P60. Evidence from mice that express the G85R SOD1 mutation indicate that TSC abnormalities are not unique for mice that express G93A SOD1 mutations. These results add to an emerging understanding that TSCs may play a role in motor terminal degeneration and denervation in animal models of motor neuron disease.

Keywords

motor neuron disease; terminal Schwann cell; neurodegeneration; motor terminal; denervation; neuromuscular junction

Corresponding author: Martin J. Pinter, Department of Physiology, Emory University School of Medicine, 615 Michael St., Atlanta, GA 30322, mpinter@emory.edu.

The authors declare no competing financial interests.

INTRODUCTION

In several animal models of motor neuron disease, degeneration begins in the periphery (Sagot et al., 1995; Balice-Gordon et al., 2000; Fischer et al., 2004). Evidence for a dissociation between motor neuron cell death and peripheral degeneration has been obtained from mice which overexpress mutations of the superoxide dismutase 1 (SOD1) protein which are found in cases of inherited ALS (Gurney et al., 1994). In these mice, inhibition of motor neuron cell death does not prevent development of muscle denervation (Gould et al., 2006). In other studies of SOD1 mice, intramuscular axonal arbors of living motor neurons have been imaged which do not innervate muscle fibers (Schaefer et al., 2005). These observations show that loss of motor unit function and weakness do not develop as a result of motor neuron cell death but rather as a result of peripheral degeneration.

The mechanisms which underlie this initial peripheral involvement are unknown. One possibility that has been considered is that normal interactions between muscle and motor neurons are disrupted. There is mixed evidence for a role of muscle-specific expression of mutant protein in determining disease phenotype in SOD1 mice with some studies suggesting a toxic influence (Sugiura et al., 2004; Wong and Martin, 2010) while others report that SOD1-expressing muscle exerts no influence on disease (Miller et al., 2006). Evidence obtained using whole muscle, syngeneic grafts to create surgical chimeras does not support a role for SOD1 muscle. We found that wildtype (WT) muscle did not inhibit SOD1 motor terminal degeneration when grafted into mice that express the G93A SOD1 mutation ($SOD1^{G93A}$) and that $SOD1^{G93A}$ muscle did not cause WT motor terminal degeneration when grafted into WT mice (Carrasco et al., 2010).

During reinnervation of grafted muscles, host Schwann cells (SCs) were found to accompany regenerating axons (Carrasco et al., 2010). Thus, a possible explanation for the appearance of motor terminal degeneration when SOD1 motor axons reinnervate WT or SOD1-expressing muscle is that interactions between SCs and motor axons, both of which express mutant protein, are sufficient to cause degeneration. Consistent with this is evidence that SC-specific expression of mutated SOD1 protein (G93A) causes no pathological effects (Turner et al., 2010), Other studies have produced inconsistent evidence for a role of mutant-expressing SCs. Using the same cre-mediated strategy (P_0 cre, (Feltri et al., 1999)), separate groups found that SC-specific partial reduction of mutant SOD1 expression accelerates (Lobsiger et al., 2009) or modestly slows (Wang et al., 2012) disease progression in SOD1 mice that express the G37R or G85R mutation, respectively. The opposing results were attributed to different dismutase activities of the G37R and G85R SOD1 mutant proteins.

More recent evidence indicates that terminal Schwann cells (TSCs, or perisynaptic Schwann cells) in some SOD1 mice exhibit altered signaling linked to motor terminal action potential activity (Arbour et al., 2015). Such evidence is potentially significant because TSCs have an important but poorly understood trophic relation with motor terminals (Koirala et al., 2003; Reddy et al., 2003). No other information is available about TSCs in SOD1 mice. We therefore examined SOD1 TSCs at several ages using immunolabeling methods. The results show that TSC abnormalities are present before denervation commences in a pattern that correlates with future disease-related muscle denervation.

METHODS

Animals

Three different transgenic mouse strains of either gender were used, each on a congenic C57BL6/J background to avoid genetic modifier effects of background strain on disease expression (Heiman-Patterson et al., 2011). Most work was conducted using mice which overexpress a transgene that carries the G93A mutation of human SOD1 protein (Gurney et al., 1994). Hereafter, these mice (B6.Cg-Tg(SOD1-G93A)1Gur/J) are referred to as B6.SOD1 mice. These mice exhibit changes in motor performance at about 50 days which are detectable by gait analysis but survive about 1 month longer (50% survival ~160 days) than the original mice carrying the same transgene on a mixed B6SJL background (Wooley et al., 2005; Heiman-Patterson et al., 2011). In some experiments, mice were used that express the human transgene for the G85R SOD1 mutation (B6.Cg-Tg(SOD1*G85R)148Dwc/J, hereafter $SOD1^{G85R}$). These mice express mutant SOD1 protein at much lower levels than $SOD1^{G93A}$ mice, and have a later disease onset (8–10 months) followed by uniformly rapid disease progression (Bruijn et al., 1997). Aged-matched C57BL6/J (hereafter WT) mice were used as controls. All mice were bred at Emory University or acquired from The Jackson Laboratory (www.jax.org, Bar Harbor, ME). All experiments were carried out in accordance with the Institutional Animal Care and Use Committees of Emory University.

Immunolabeling

Under general anesthesia, the medial gastrocnemius (MG) and soleus muscles were recovered and prepared for immunolabeling. Muscles were placed into 4% paraformaldehyde for 1 hr. Muscles were washed in a 0.1 M phosphate buffered solution (PBS) and incubated at 4°C overnight in PBS containing 20% sucrose for cryoprotection. Sections (50 μm thickness) were obtained using a Cyrostat (Leica). Motor endplate acetylcholine receptors (AChRs) were labeled with Alexa 488 conjugated α-bungarotoxin (Molecular Probes). Axons and motor terminals (synaptic vesicles) were labeled with a mouse monoclonal antibody against the phosphorylated heavy fragment of neurofilament protein (SMI31, 1:400, Sternberger Monoclonal) and synaptic vesicles (SV2, 1:20, Developmental Studies Hybridoma Bank). Labeling was visualized using Cy5-conjugated secondary antibody (1:100, Jackson Immunoresearch Laboratories). Schwann cells (SCs) were labeled with a rabbit polyclonal antibody against S100B Ca^{2+}-binding protein (S100, 1:100, Dako) and visualized using a rhodamine-conjugated secondary antibody (1:100, Jackson Immunoresearch Laboratories). In addition to S100 labeling, SCs in some sections were also labeled with a goat polyclonal antibody against the low affinity nerve growth factor receptor p75 (NGFR p75, 1:50, Santa Cruz SC-6188) and visualized using a Cy5-conjugated secondary antibody (1:100, Jackson Immunoresearch Laboratories). DAPI staining was used to identify SC or TSC cell body nuclei. This staining was performed as per manufacturer's instructions using slide mounting media (Vectashield) which included DAPI.

Imaging

Z-axis stacks of images of neuromuscular junctions (NMJs) were obtained at sequential focal planes (1.0 μm separation) using an upright microscope equipped with a motorized stage (Leica). Stacks were deconvolved using a commercially available inverse filter algorithm (ImagePro). In some cases, stacks of confocal images were obtained.

Analysis

Images of NMJs were analyzed at high magnification (100x) to determine the extent to which presynaptic SMI+SV2 labeling overlaid postsynaptic labeling for AChRs in superimposed images. SMI+SV2 labeling was used to assign the following categories of endplate innervation; endplates that exhibited a complete absence of SMI+SV2 labeling were considered to be denervated; endplates that showed SMI+SV2 labeling present in all ACHR-rich endplate arms or branches were considered to be innervated; endplates that showed SMI+SV2 labeling present in some but not all ACHR-rich arms or branches were considered to be partially innervated. For analysis, randomly selected fields of NMJs were first located at low magnification. Then, at high magnification all the NMJs in each field were categorized as described above. The extent of endplate S100 coverage was also assessed at 100x magnification and assigned into 3 categories (full, partial, absent). Additional analyses to assess colabeling for P75, S100 and DAPI labeling at 100x magnification were performed as described in Results. Unless noted otherwise, all NMJ measurements were sampled from 80 NMJs per muscle, and only one MG-soleus pair from the same side was sampled per animal.

TSC cell bodies were identified by S100 and DAPI nuclear colabeling (Love and Thompson, 1998). As shown in Fig 1, multiple DAPI-labeled nuclei are located in the vicinity of the NMJ, so TSC cell body identification needs to be performed with care. To identify TSC cell bodies, multiple focal planes were viewed using a 100x, oil-immersion objective with a variable aperture closed down to minimize depth of focus. At each focal plane, the appropriate fluorescence filters were manually switched while viewing images on a video monitor to ensure that S100 and DAPI labeling were located in identical focal planes. Since some time was needed to accomplish these views, mercury lamp illumination was used to minimize the amount of light exposure. In most cases, these steps were sufficient to either identify TSC cell bodies or to exclude their presence. In more difficult cases, full image stacks of DAPI and S100 labeling were taken to enable finer scrutiny of labeling placement.

Statistics

Two-way contingency tables were used to determine effects of genotype (B6.SOD1 v WT), age or treatment on frequency distributions of categorical variable means describing innervation status (SMI-SV2 labeling), NMJ S100 and P75 labeling coverage, and S100-P75 colabeling status. For comparing average values, nested analysis of variance was used. Tukey's honestly significant difference post-hoc test was used to test the significance of differences between WT, contralateral control and B6.SOD1 average values. All analysis was performed using commercially available software (Systat Inc). Mean values are presented ± 1 SEM.

RESULTS

Previous studies have shown that in SOD1^{G93A} mice, denervation and motor unit dysfunction appear first in muscles that contain fast-type motor units (Frey et al., 2000; Pun et al., 2006; Hegedus et al., 2007). In the gastrocnemius muscles, denervation was found to commence first on fibers belonging to type FF units, while fibers belonging to type S or slow units appeared more resistant to denervation (Frey et al., 2000). In order to learn whether TSC changes appear in a similar pattern, we compared TSC morphology and number between NMJs in medial gastrocnemius (MG) and soleus muscles at P30 and at P60. By P30, the mouse MG is dominated by fibers expressing myosin heavy-chain 2B (which populate type FF units) but lacks type I fibers which populate type S motor units. Soleus possesses about 50% type I fibers but lacks 2B fibers (Agbulut et al., 2003). Thus, differences specific for type FF or for type S units should be revealed by comparing data between the MG and soleus muscles.

P30 SOD1 MG NMJs lack TSCs

Innervation and S100 labeling status were first examined in P30 B6.SOD1 mice. This age was selected in part because it occurs well before motor symptoms are first detected in B6.SOD1 mice (ca P50, (Wooley et al., 2005). In addition, the early postnatal survival dependence of TSCs and proximal SCs on innervation has mostly disappeared by P30 (Hayworth et al., 2006) and postnatal synapse elimination is normally complete (Sanes and Lichtman, 1999; Sanes and Lichtman, 2001). In P30 B6.SOD1 soleus and MG muscles, we found that 100% of NMJs were fully innervated by a single motor axon as judged by SMI-SV2 labeling and that NMJs were completely covered by S100 labeling. In these respects, B6.SOD1 NMJs were statistically indistinguishable from soleus and MG NMJs in P30 WT muscles (Pearson chi square, $p > 0.05$). Moreover, B6.SOD1 muscles possessed typical pretzel-shaped motor endplates. These shapes are thought to occur as a result of synaptic competition which underlies elimination of polyneuronal innervation present at early neonatal periods (Sanes and Lichtman, 1999; Sanes and Lichtman, 2001). Together with uniform single innervation of NMJs, these results suggest that postnatal synapse elimination proceeded normally in these B6.SOD1 muscles.

Other aspects of B6.SOD1 NMJs, however, differed from normal. In B6.SOD1 MG muscles, combined S100/DAPI labeling showed that many NMJs lacked TSC cell bodies despite being fully innervated and 100% covered by S100 labeling. Instead, many MG NMJs were covered by processes that arose from SCs whose cell bodies were located along the preterminal axon. Two examples of this type of NMJ are shown in Fig 1A–B. This type of NMJ was never encountered in WT P30 MG muscles where NMJs uniformly possessed one or more TSC cell body. An example of such an endplate from a P30 WT MG muscle is shown in Fig 1C. Using S100/DAPI colabeling, TSC cell bodies were identified at NMJs and counted. Histograms of TSC cell body counts showed that almost 50% of P30 B6.SOD1 MG NMJs lacked TSC cell bodies whereas all WT MG NMJs had one or more TSC cell body (Fig 2). Because many NMJs lacked TSC cell bodies, the overall average number of TSC cell bodies at P30 B6.SOD1 MG NMJs (0.65 ± 0.03) was significantly less that the WT average (1.37 ± 0.03, nested ANOVA, $p < 0.01$, $N = 4$ muscles in each group).

Another feature that differed between P30 B6.SOD1 and WT MG NMJs was the placement of TSC cell bodies. Many TSCs cell bodies which were located at fully innervated P30 SOD1 MG NMJs were positioned differently from WT and showed a tendency to be located outside the perimeter of endplate ACHR labeling. Fig 3A1 shows examples of TSC placement at a P30 WT MG NMJ. In this case, the leftmost TSC cell body aligns along adjacent S100+ arms. The image of the associated endplate was processed to detect the edges of ACHR labeling. The result is shown superimposed over S100 labeling in Fig 3A2 where it may be seen that the majority of the leftmost TSC cell body is contained within the limits of endplate ACHR labeling. This placement was found for the majority (> 90%) of WT MG TSC cell bodies (Fig 3D) and will be described here as normal placement. Most of the TSC cell body located on the right in Fig 3A2, however, was located just beyond the perimeter of ACHR labeling, and thus appeared displaced relative to the majority of WT cell bodies. While this positioning was only found in a minority (9%) of P30 WT MG NMJs, displaced TSC cell bodies were found in a large fraction (45%) of P30 B6.SOD1 MG NMJs (Fig 3D). An example in which 2 TSC cell bodies were displaced just outside the perimeter of ACHR labeling is shown in Fig 3B. In another case, one TSC cell body was displaced (Fig 3C, right TSC) while the other was positioned normally (left TSC). Overall, the distribution of TSC cell body placement at P30 B6.SOD1 MG NMJs differed significantly from the P30 WT distribution (Fig 3D, Pearson chi square, $p < 0.01$). These results show that in the P30 B6.SOD1 MG, many NMJs lack TSCs while many TSCs present at other NMJs have cell bodies abnormally placed relative to WT.

P30 soleus

P30 B6.SOD1 soleus NMJs exhibited significantly less evidence of TSC abnormalities than did MG NMJs. Similar to MG, all B6.SOD1 soleus NMJs were fully innervated and 100% covered by S100 labeling. Some B6.SOD1 soleus NMJs were found which lacked TSC cell bodies, but the mean fraction (ca 5%, N = 4 muscles) was much less than in the B6.SOD1 MG muscle (Fig 4A). Counts of TSC cell bodies showed that the average number at B6.SOD1 soleus NMJs (1.38 ± 0.03) was not significantly different than the P30 WT average at NMJs of P30 WT soleus muscles (1.44 ± 0.03, nested ANOVA, $p > 0.05$, N = 4 muscles in each group). As with P30 SOD1 MG NMJs, there was a tendency for displaced TSC cell bodies but overall TSC location was not significantly different from P30 WT soleus NMJs (Fig 4B, Pearson chi square, $p > 0.05$). It should also be noted that average values for WT mouse soleus TSC per NMJ reported here are less than those reported by others for mice a similar age (Lee et al., 2011, mean = 3.6, age = P13; Darabid et al., 2013, mean = 2.7, age = P8). The latter studies used mice on genetic backgrounds that differ from the present study and analyzed whole muscle rather than muscle sections (as in the present study) to derive TSC per NMJ average values. The extent to which these factors and other possible differences in methods contribute to variation of TSC counts between studies has yet to be established.

P30 summary

The results demonstrate that before any disease-related denervation occurs in B6.SOD1 MG and soleus muscles, abnormalities appear in the organization and number of TSCs. The

results show that these abnormalities are considerably more extensive in the B6.SOD1MG than in the B6.SOD1 soleus muscle.

P60 SOD1 NMJs

To learn how subsequent innervation status at SOD1 NMJs might be related to P30 status, we studied innervation and S100 labeling status at P60 SOD1 NMJs. In previous studies, we found that by P70-90, B6.SOD1 hindlimb muscles exhibit a mixture of fully and partially innervated NMJs as well as denervated NMJs (Carrasco et al., 2010; Carrasco et al., 2012). In the present study, B6.SOD1 MG and soleus muscles were found to contain this mixture of innervation status by P60 and that SOD1 soleus NMJs were considerably less affected than SOD1 MG NMJs.

Innervation

The innervation status of P60 NMJs was classified into fully-innervated, partially-innervated and denervated categories based on examination (100x) of SMI-SV2 labeling, as described previously (Carrasco et al., 2010; Carrasco et al., 2012). Figs 5A–B show the distributions of average innervation status for P60 SOD1 MG (N = 10) and soleus NMJs (N = 4). At P60, the majority (mean, 64 ± 2.3%) of SOD1 MG NMJs were fully-innervated but significant fractions were either partially-innervated (12 ± 2%) or denervated (24 ± 3%, Fig 5A). Denervated (mean, < 1%) and partially innervated (3.5 ± 1.6%) NMJs occurred at a considerably lower frequency in SOD1 soleus muscles which were populated primarily (96.0 ± 1.5%) by fully innervated NMJs. Statistical analysis showed that the proportions of the 3 innervation categories of P60 SOD1 MG and soleus NMJs differed significantly from both P30 B6.SOD1 and from P60 WT NMJs, 100% of the latter being fully-innervated (Pearson chi square, $p > 0.01$; N as above for P60 B6.SOD1 muscles, N = 4 for P60 WT muscles and for P30 B6.SOD1 muscles). These results demonstrate the progression of disease between P30 and P60 in terms of increased incidence of NMJ denervation, and show that this progression is greater at MG than at soleus NMJs.

S100 coverage

A parallel assessment of S100 labeling was performed in P60 B6.SOD1 muscles for each NMJ at which innervation status was assessed. Overall, S100 labeling at SOD1 NMJs was found to be directly related to innervation status. For both P60 B6.SOD1 soleus (N = 4) and MG B6.SOD1 (N = 10) muscles, 100% of fully innervated NMJs were also fully covered by S100 labeling. An example of this type of S100 labeling coverage is shown in Fig 5C. An identical innervation-S100 labeling correspondence was also found for partially innervated and denervated NMJs. Examples of these types of S100 labeling coverage are shown in Fig 5D. Contingency table analysis showed that the association between categories of NMJ innervation status and NMJ S100 coverage was statistically significant (Pearson chi-square, $p < 0.01$). Thus, fully and partially innervated SOD1 NMJs possessed corresponding S100 labeling coverage, while denervated NMJs (found primarily in P60 SOD1 MG) lacked S100 labeling altogether. Because of the relationship between S100 coverage and innervation, histograms depicting the distribution of innervation categories (Fig 5A, B) also represent S100 coverage status distributions.

Another feature of denervated SOD1 NMJs is illustrated in Fig 5C. In this case, it may be seen that, in addition to an absence of NMJ S100 labeling, no S100 labeling is evident in the immediate vicinity of the NMJ. A lack of preterminal S100 labeling was observed at 100% of denervated B6.SOD1 MG NMJs. In contrast, fully or partially innervated MG NMJs always had evidence of presynaptic S100 labeling associated with the preterminal motor axon (cf, Fig 5C and partially-innervated NMJ in Fig 5D). These results demonstrate that a lack of S100 labeling at denervated B6.SOD1 NMJs is not specific for the NMJ and includes an absence of S100 labeling in preterminal areas.

Specificity of S100 absence

To determine whether the absence of S100 labeling at denervated P60 SOD1 MG NMJs is specific for S100, muscle sections were colabeled for P75. P75 labeling is not normally found at innervated NMJs but appears after denervation in normal TSCs and preterminal SCs (Reynolds and Woolf, 1992; O'Malley et al., 1999). In P60 B6.SOD1 MG muscles (N = 4), P75 and S100 labeling were examined at NMJs and in preterminal regions. In 3/4 muscles, P75 labeling was found at a small number of partially innervated NMJs (mean, 7.5% of NMJs) and this P75 labeling colocalized with S100 labeling. Examples of this labeling are shown in Fig 6A–B for 2 MG NMJs with different degrees of partial S100 coverage. No P75 labeling was found at other NMJs including those which were completely covered by S100 labeling (fully innervated) and those that completely lacked S100 labeling (denervated). An example is shown in Fig 6C1–2 of an MG NMJ which was completely covered by S100 labeling provided by a resident TSC (verified by DAPI colabeling, not shown) which did not express P75. Given the association between NMJ innervation and S100 coverage described above, these results show that, as expected, fully innervated P60 B6.SOD1 MG NMJs which are fully covered by S100 labeling do not express P75. However, denervated NMJs which do not label for S100 also do not label for P75. Thus, denervated B6.SOD1 MG NMJs lack P75 as well as S100 labeling.

Because of the presence of denervated NMJs at P60, some P75 labeling observed in the B6.SOD1 MG may belong to regenerating axons. Thus, it is unclear whether all B6.SOD1 TSCs are capable of expressing P75. P75 labeling appears in normal TSCs and SCs following block of neuromuscular transmission by botulinum toxin (BOTX, (Hassan et al., 1994). Previous studies showed that BOTX blockade causes the appearance of P75 labeling at some SOD1 NMJs (Frey et al., 2000) et al), but how this labeling is related to innervation status and S100 colabeling was not examined. BOTX (type A, 0.5 mouse LD50 per muscle) was therefore injected into P60 B6.SOD1 MG muscles (N = 3). After 4d, paralysis was verified by the absence of any visible contractions viewed under a dissecting microscope following electrical stimulation of the MG nerve. NMJ innervation status, S100 coverage and S100-P75 colabeling were then examined. Analysis showed that BOTX paralysis did not affect the distributions of either innervation status or S100 NMJ coverage; in both cases, the distributions did not differ significantly from the corresponding distributions from untreated P60 B6.SOD1 MG muscles (Pearson chi square, $p > 0.05$). This is consistent with other reports that BOTX applied for up to 3 days has no effects on several morphological features of TSCs (Brill et al., 2011). NMJ and preterminal P75 labeling appeared following BOTX paralysis, and the distribution of P75 labeling closely mirrored NMJ S100 coverage

status. Thus, an average of about 75% of NMJs that were classified as having full S100 coverage also possessed full P75 colabeling (example, Fig 6D) whereas NMJs at which no S100 labeling could be identified had no detectable P75 colabeling. The remainder of NMJs that were classified as having full S100 endplate coverage (ca 25%) showed an absence of P75 labeling over the endplate (Fig 6E). However, in over half of these cases (57%), S100-P75 colabeling was observed overlying preterminal axons. These cases may arise from the inevitable variability of BOTX levels within the injected muscle volume which can produce an absence of or partial release blockade at some NMJs (Pinter et al., 1991). These results show that B6.SOD1 TSCs and SC processes that express S100 are also capable of expressing P75 after BOTX. The results also show that P75 labeling does not appear after BOT at NMJs which lack S100 labeling. Since other B6.SOD1 TSCs and SCs are able to maintain S100 and express P75 after BOTX, the results suggest that denervated B6.SOD1 NMJs may lack TSCs or SC processes or that TSCs which are present are incapable of expressing both S100 and P75.

P60 TSC cell bodies

The absence of S100 labeling at some MG NMJs prevented counting of TSC cell bodies at all P60 NMJs because identifying TSC cell bodies depends on S100/DAPI colabeling. TSC number was therefore evaluated only at NMJs that were fully or partially covered by S100 labeling. In P60 SOD1 MG, this count had a mean value (0.59 ± 0.02, N = 10 muscles) which was significantly less than TSC cell body counts from P60 WT MG NMJs (1.49 ± 0.04, N = 4 muscles, nested ANOVA, $p < 0.01$) but not significantly different from the mean P30 MG TSC cell count (0.65 ± 0.03, N = 4 muscles, $p > 0.05$). Overall at P60, a mean of about 36% of fully S100-covered B6.SOD1 MG NMJs had no TSC cell body, while 35% had one or more TSC cell body (Fig 7A). In terms of NMJ TSC number, these results show that the P60 SOD1 MG NMJ population that is fully covered by S100 labeling is similar to the overall P30 SOD1 MG NMJ population, despite the emergence of significant denervation at P60.

P60 soleus

Unlike P60 B6.SOD1 MG, most soleus NMJs were fully innervated (96.0% ± 1.5, N = 4 muscles) with only small fractions partially innervated (3.5%) or denervated (0.5%). In addition, fully innervated NMJs were also fully covered by S100 labeling. In contrast to P30 B6.SOD1 soleus NMJs, a minority of P60 soleus NMJs (7%) lacked TSC cell bodies and were fully covered by S100 labeling (Fig 7B). Limiting comparison only to fully S100-covered NMJs, analysis showed that the mean TSC cell body count for P60 B6.SOD1 soleus NMJs (1.21 ± 0.04, N = 4 muscles) differed significantly from both P60 WT soleus NMJs (1.52 ± 0.06, N = 4 muscles, $p < 0.01$) and from P30 B6.SOD1 NMJs (1.44 ± 0.03, N = 4 muscles, $p < 0.01$). These results demonstrate that by P60, B6.SOD1 soleus NMJs have begun exhibiting the same disease manifestations that are already present by P30 and to a greater extent by P60 at B6.SOD1 MG NMJs.

G85R SOD1 mice

To determine if the present findings are specific for the G93A SOD1 mutation, we examined innervation status, S100 coverage and TSC cell body number in MG muscles of 160d G85R SOD1 mice (N = 2) and compared results with data from 6 mo WT MG NMJs. In WT MG (N =3), all NMJs were found to be fully innervated and covered by S100 labeling and that all NMJs had one or more TSC cell bodies. Almost all G85R MG NMJs (97%) were completely innervated as well as covered by S100 labeling (Fig 8A). However, G85R MG NMJs featured a significant fraction which did not have TSC cell bodies (Fig 8B). As a result, the average number of TSC cell bodies at G85R MG NMJs was significantly lower than WT MG (Fig 8C). These results indicate that an absence of TSC cell bodies appears prior to significant denervation at G85R MG NMJs and that the absence of TSC cell bodies at SOD1 NMJs is not specific for the G93A mutation. Moreover, since expression levels of G85R mutant protein are 0.2 -1X endogenous expression levels (Bruijn et al., 1997), these results indicate that the much higher expression levels of mutant protein typical of G93A mutant mice (~ 20x endogenous levels, (Gurney et al., 1994) are not necessary for the appearance of these TSC abnormalities.

DISCUSSION

The results of this study show that TSC disorganization is present well before motor terminal (MT) degeneration and denervation commence in B6.SOD1 mice. This disorganization appears as an absence of TSCs at many P30 MG NMJs, with NMJs covered instead by processes of SCs whose cell bodies are located along preterminal axons. Disorganization is also shown by displacement of TSC cell bodies at other MG and soleus NMJs. The evidence shows that these features are more pronounced in MG than in soleus muscles at P30, and that this difference predicts the extent of denervation difference between these muscles at P60. Results obtained from mice that express the G85R SOD1 mutation indicate that the TSC disorganization found in G93A mice does not depend on the genotype of SOD1 mutation or on known differences of dismutase activity between the mutant proteins. Although a direct connection between abnormal TSC coverage at P30 and denervation at P60 remains to be established, these results suggest that TSCs may play a previously unrecognized role in the loss of innervation and progression of disease in SOD1 mice.

An important question is how the abnormal SC coverage of P30 B6.SOD1 MG NMJs might lead to subsequent MT degeneration. P30 WT MG NMJs normally average more than 1 TSC per endplate (Fig 2). Studies show that TSCs are organized in a tile-like manner such that the territories of MT coverage do not overlap. TSCs thus form a functional group that is physically isolated from the preterminal SC such that no SC processes span the intervening heminode (Brill et al., 2011). These observations suggest that physically- and functionally-separated preterminal SC and terminal TSC compartments normally exist at the NMJ. Release of ACh and ATP from MTs produces Ca2+ signals in TSCs which appear to be greatest in the nearby TSC cell bodies. TSCs thus monitor MT activity and are thought to engage in reciprocal signaling with the underlying MT (Rochon et al., 2001; Todd et al., 2010), and the normal structural features of TSCs suggest that this signaling is likely

confined to TSCs. It seems likely that this signaling and any dependent processes would be disrupted if NMJs are covered by processes derived from a remotely located SC; at the very least, activity-related Ca2+ signals could be subject to additional diffusion and decrement before reaching the remote SC cell body. Recent evidence indicate that TSC Ca2+ signaling is increased at some NMJs in the soleus muscle of G137R SOD1 mice before denervation commences (Arbour et al., 2015). Whether these or other versions of signaling abnormality are associated with the type of morphological changes seen at B6.SOD1 MG NMJs has yet to be determined.

Another possible consequence of abnormal TSC/SC MT coverage in B6.SOD1 is suggested by functional/structural features of normal axons. Myelinated axons have a spatially specific distribution of ion channels, and evidence from several sources indicates that SCs are involved in specifying and maintaining this channel arrangement (Vabnick et al., 1997; Vabnick and Shrager, 1998). In demyelination of multiple sclerosis (MS), Na+ channels appear in demyelinated internode regions which can produce abnormally large inward currents which may promote degeneration (Craner et al., 2004a; Craner et al., 2004b). The normal mouse motor terminal also has a spatially-specific arrangement of ion channels; voltage-gated Na+ channels are located at high density specifically in the heminode (preterminal axon) but at much lower density within the terminal proper. Fast kinetic K+ channels are located in the terminals along with Ca2+ channels (Brigant and Mallart, 1982). How this organization is normally maintained is not known. However, incorporating new evidence from TSC studies (Brill et al., 2011), it appears that Na+ channels are mostly excluded from and K+/Ca2+ channels are admitted into MT regions which are normally covered by multiple TSC cell bodies and processes. Based on this, it is tempting to speculate that TSCs may influence the organization of MT ion channels as the myelinating SC influences axonal ion channel organization. If this notion is correct, then the TSC alterations we now find at SOD1 endplates might have consequences for MT ionic channel distribution that place the MT at risk for degenerative changes in a manner not unlike that envisioned for demyelinated MS axons.

A final possible functional consequence is raised by our results from denervated control B6.SOD1 MG NMJs. S100 labeling was completely absent over these NMJs as well as in preterminal regions (Fig 5), and no P75 labeling was observed as is found at denervated, normal NMJs (Reynolds and Woolf, 1992). In addition, P75 labeling did not appear at these NMJs after BOTX paralysis whereas P75 labeling appeared at NMJs that also possessed S100 labeling and thus TSCs or SC processes. One possible explanation for these results is that TSCs and/or SC processes which are located at denervated B6.SOD1 NMJs (and in preterminal regions) have both ceased to produce S100 and fail to express P75 after BOTX treatment, in contrast with B6.SOD1 TSCs and SC processes at innervated NMJs. In this case, B6.SOD1 TSCs and preterminal SCs exhibit abnormal behavior at denervated NMJs. An alternative explanation is that TSCs and/or SC processes have vacated denervated B6.SOD1 NMJs. Particularly if the latter possibility is correct, serious consequences for compensatory reinnervation of denervated NMJs may result. Because they provide necessary growth paths, TSCs at denervated endplates are required for reinnervation by nearby terminal sprouts (Son et al., 1996; Love and Thompson, 1999). If TSCs are absent

from ***denervated*** SOD1 NMJs, then these NMJs cannot be reinnervated by terminal sprouting, even though MTs at nearby innervated NMJs may be able to produce such sprouts. The overall effect will be to speed the development of weakness. Low MT sprouting competence has been noted in $SOD1^{G93A}$ mice but attributed to disease expression in motor neurons (Frey et al., 2000; Gould et al., 2006; Pun et al., 2006). Our findings support the alternative possibility that this may be a property of abnormal TSCs. The only reinnervation option available during disease progression is likely to be nodal sprouting from nearby surviving motor axons (Lubischer and Thompson, 1999). In support of this, imaging studies have reported the presence of nodal but not terminal sprouts in SOD1 muscles (Schaefer et al., 2005).

Post-natal NMJ development

All P30 B6.SOD1 NMJs were innervated by a single axon which shows that postnatal synapse elimination concluded normally. This argues against a generalized effect on NMJ postnatal development produced by the B6.SOD1 disease process. However, many B6.SOD1 MG NMJs lack TSCs while the remaining MG NMJs and all soleus NMJs have at least 1 TSC cell body at P30. This suggests that a more selective interaction exists between the disease process and NMJ development. Normally, many NMJs lack TSCs at birth and are instead covered by processes of SCs with cell bodies located in the preterminal axon. During the next 2 weeks, average TSC number increases significantly at normal NMJs, the result of an initial seeding by migration of SC cell bodies from preterminal locations followed by mitosis (Love and Thompson, 1998). It may be that such migration stalls along certain B6.SOD1 MG axons or that TSCs abandon NMJs.

A more general question is why TSC abnormalities associate to a greater extent with P30 MG than with soleus muscles. Earlier studies have shown that muscle fibers belonging to type FF motor units become denervated before other fiber types in adult $SOD1^{G93A}$ mice (Frey et al., 2000; Pun et al., 2006). By 2–3 weeks postnatal, the normal gastrocnemius muscle in mice is dominated by type 2B fibers (which populate type FF units) whereas the soleus muscle lacks 2B fibers (Agbulut et al., 2003). It is thus likely that TSC abnormalities also appear first in type FF units, but questions remain about other factors that may be associated with the MG-soleus difference in TSC disorganization. During the first postnatal month, adult activity pattern differences emerge between fast and slow muscles like the MG and soleus (Navarrete and Vrbova, 1983; Personius and Balice-Gordon, 2001; Buffelli et al., 2002). Associated with the emergence of these patterns are changes of MT synaptic release properties that are thought to be adaptations to the emergent adult activity patterns (Bewick et al., 2004). Thus, quantal content becomes greater at NMJs of fast muscles like the MG, a property thought to provide synaptic transmission reliability during the high frequency action potential trains typical of fast motor units (Reid et al., 1999). The presynaptic changes which occur after synapse elimination completes and achieve this fast-slow difference in quantal content are most pronounced at NMJs of fast muscles (Bewick et al., 2004). Whether this aspect of synaptic function plays a role in determining TSC disorganization at B6.SOD1 MG NMJs or whether TSC disorganization affects these adaptations will require further investigation.

Cell type dependence

A closely related question is whether TSC/SC abnormalities at B6.SOD1 NMJs arise as a result of mutant protein expression in TSCs/SCs, motor terminals/axons or both. The present study provides no answer to this question. However, a previous study of the effects of SC-specific inhibition of mutant SOD1 included images of NMJs that bear a striking resemblance to those shown in Fig 1 A,B (Lobsiger et al., 2009). Thus, no apparent TSC cell bodies can be seen along S100-labeled processes that clearly overlie endplates whereas prominent SC nuclei are located more proximally along preterminal axons and express markers indicating inhibition of SOD1 (G37R mutant) expression (Fig 3C,(Lobsiger et al., 2009). Such evidence suggests that TSC disorganization in number and placement may not depend on mutant protein expression in SCs but rather on expression in motor terminals or axons. If this is correct, then it may be that TSC disorganization arises from altered signaling between MTs and TSCs (Rochon et al., 2001; Todd et al., 2010; Arbour et al., 2015). Alterations such as this may involve extracellular molecular paths that are accessible to exogenous therapeutics. Additional efforts will be needed to identify such interactions.

Acknowledgments

The authors wish to thank Drs. Mark Rich and Greg Cox for helpful discussions. This work was supported by NIH grant NS074231.

References

Agbulut O, Noirez P, Beaumont F, Butler-Browne G. Myosin heavy chain isoforms in postnatal muscle development of mice. Biol Cell. 2003; 95:399–406. [PubMed: 14519557]

Arbour D, Tremblay E, Martineau E, Julien JP, Robitaille R. Early and persistent abnormal decoding by glial cells at the neuromuscular junction in an ALS model. J Neurosci. 2015; 35:688–706. [PubMed: 25589763]

Balice-Gordon RJ, Smith DB, Goldman J, Cork LC, Shirley A, Cope TC, Pinter MJ. Functional motor unit failure precedes neuromuscular degeneration in canine motor neuron disease. Ann Neurol. 2000; 47:596–605. [PubMed: 10805330]

Bewick GS, Reid B, Jawaid S, Hatcher T, Shanley L. Postnatal emergence of mature release properties in terminals of rat fast- and slow-twitch muscles. Eur J Neurosci. 2004; 19:2967–2976. [PubMed: 15182303]

Brigant JL, Mallart A. Presynaptic currents in mouse motor endings. J Physiol. 1982; 333:619–636. [PubMed: 6304288]

Brill MS, Lichtman JW, Thompson W, Zuo Y, Misgeld T. Spatial constraints dictate glial territories at murine neuromuscular junctions. J Cell Biol. 2011; 195:293–305. [PubMed: 22006952]

Bruijn LI, Becher MW, Lee MK, Anderson KL, Jenkins NA, Copeland NG, Sisodia SS, Rothstein JD, Borchelt DR, Price DL, Cleveland DW. ALS-linked SOD1 mutant G85R mediates damage to astrocytes and promotes rapidly progressive disease with SOD1-containing inclusions. Neuron. 1997; 18:327–338. [PubMed: 9052802]

Buffelli M, Busetto G, Cangiano L, Cangiano A. Perinatal switch from synchronous to asynchronous activity of motoneurons: link with synapse elimination. Proc Natl Acad Sci U S A. 2002; 99:13200–13205. [PubMed: 12242340]

Carrasco DI, Bichler EK, Seburn KL, Pinter MJ. Nerve terminal degeneration is independent of muscle fiber genotype in SOD1 mice. PLoS One. 2010; 5:e9802. [PubMed: 20339550]

Carrasco DI, Bichler EK, Rich MM, Wang X, Seburn KL, Pinter MJ. Motor terminal degeneration unaffected by activity changes in SOD1(G93A) mice; a possible role for glycolysis. Neurobiol Dis. 2012; 48:132–140. [PubMed: 22750521]

Craner MJ, Hains BC, Lo AC, Black JA, Waxman SG. Co-localization of sodium channel Nav1.6 and the sodium-calcium exchanger at sites of axonal injury in the spinal cord in EAE. Brain. 2004a; 127:294–303. [PubMed: 14662515]

Craner MJ, Newcombe J, Black JA, Hartle C, Cuzner ML, Waxman SG. Molecular changes in neurons in multiple sclerosis: altered axonal expression of Nav1.2 and Nav1.6 sodium channels and Na+/Ca2+ exchanger. Proc Natl Acad Sci U S A. 2004b; 101:8168–8173. [PubMed: 15148385]

Darabid H, Arbour D, Robitaille R. Glial cells decipher synaptic competition at the mammalian neuromuscular junction. J Neurosci. 2013; 33:1297–1313. [PubMed: 23345206]

Feltri ML, D'Antonio M, Previtali S, Fasolini M, Messing A, Wrabetz L. P0-Cre transgenic mice for inactivation of adhesion molecules in Schwann cells. Ann N Y Acad Sci. 1999; 883:116–123. [PubMed: 10586237]

Fischer LR, Culver DG, Tennant P, Davis AA, Wang M, Castellano-Sanchez A, Khan J, Polak MA, Glass JD. Amyotrophic lateral sclerosis is a distal axonopathy: evidence in mice and man. Exp Neurol. 2004; 185:232–240. [PubMed: 14736504]

Frey D, Schneider C, Xu L, Borg J, Spooren W, Caroni P. Early and selective loss of neuromuscular synapse subtypes with low sprouting competence in motorneuron diseases. J Neurosci. 2000; 20:2534–2542. [PubMed: 10729333]

Gould TW, Buss RR, Vinsant S, Prevette D, Sun W, Knudson CM, Milligan CE, Oppenheim RW. Complete dissociation of motor neuron death from motor dysfunction by Bax deletion in a mouse model of ALS. J Neurosci. 2006; 26:8774–8786. [PubMed: 16928866]

Gurney ME, Pu H, Chiu AY, Dal Canto MC, Polchow CY, Alexander DD, Caliendo J, Hentati A, Kwon YW, Deng HX, Chen W, Zhai P, Sufit RL, Siddique T. Motor neuron degeneration in mice that express a human Cu,Zn superoxide dismutase mutation. Science. 1994; 264:1772–1775. [PubMed: 8209258]

Hassan SM, Jennekens FG, Veldman H, Oestreicher BA. GAP-43 and p75NGFR immunoreactivity in presynaptic cells following neuromuscular blockade by botulinum toxin in rat. J Neurocytol. 1994; 23:354–363. [PubMed: 8089707]

Hayworth CR, Moody SE, Chodosh LA, Krieg P, Rimer M, Thompson WJ. Induction of neuregulin signaling in mouse schwann cells in vivo mimics responses to denervation. J Neurosci. 2006; 26:6873–6884. [PubMed: 16793894]

Hegedus J, Putman CT, Gordon T. Time course of preferential motor unit loss in the SOD1 G93A mouse model of amyotrophic lateral sclerosis. Neurobiol Dis. 2007; 28:154–164. [PubMed: 17766128]

Heiman-Patterson TD, Sher RB, Blankenhorn EA, Alexander G, Deitch JS, Kunst CB, Maragakis N, Cox G. Effect of genetic background on phenotype variability in transgenic mouse models of amyotrophic lateral sclerosis: a window of opportunity in the search for genetic modifiers. Amyotroph Lateral Scler. 2011; 12:79–86. [PubMed: 21241159]

Koirala S, Reddy LV, Ko CP. Roles of glial cells in the formation, function, and maintenance of the neuromuscular junction. J Neurocytol. 2003; 32:987–1002. [PubMed: 15034281]

Lee YI, Mikesh M, Smith I, Rimer M, Thompson W. Muscles in a mouse model of spinal muscular atrophy show profound defects in neuromuscular development even in the absence of failure in neuromuscular transmission or loss of motor neurons. Dev Biol. 2011; 356:432–444. [PubMed: 21658376]

Lobsiger CS, Boillee S, McAlonis-Downes M, Khan AM, Feltri ML, Yamanaka K, Cleveland DW. Schwann cells expressing dismutase active mutant SOD1 unexpectedly slow disease progression in ALS mice. Proc Natl Acad Sci U S A. 2009; 106:4465–4470. [PubMed: 19251638]

Love FM, Thompson WJ. Schwann Cells Proliferate at Rat Neuromuscular Junctions during Development and Regeneration. J Neuroscience. 1998; 18:9376–9385. [PubMed: 9801376]

Love FM, Thompson WJ. Glial cells promote muscle reinnervation by responding to activity-dependent postsynaptic signals. J Neurosci. 1999; 19:10390–10396. [PubMed: 10575036]

Lubischer JL, Thompson WJ. Neonatal partial denervation results in nodal but not terminal sprouting and a decrease in efficacy of remaining neuromuscular junctions in rat soleus muscle. J Neurosci. 1999; 19:8931–8944. [PubMed: 10516312]

Miller TM, Kim SH, Yamanaka K, Hester M, Umapathi P, Arnson H, Rizo L, Mendell JR, Gage FH, Cleveland DW, Kaspar BK. Gene transfer demonstrates that muscle is not a primary target for non-cell-autonomous toxicity in familial amyotrophic lateral sclerosis. Proc Natl Acad Sci U S A. 2006; 103:19546–19551. [PubMed: 17164329]

Navarrete R, Vrbova G. Changes of activity patterns in slow aNd fast muscles during postnatal development. Developmental Brain Research. 1983; 8:11–19.

O'Malley JP, Waran MT, Balice-Gordon RJ. In vivo observations of terminal Schwann cells at normal, denervated, and reinnervated mouse neuromuscular junctions. J Neurobiol. 1999; 38:270–286. [PubMed: 10022572]

Personius KE, Balice-Gordon RJ. Loss of correlated motor neuron activity during synaptic competition at developing neuromuscular synapses. Neuron. 2001; 31:395–408. [PubMed: 11516397]

Pinter MJ, Vanden Noven S, Muccio D, Wallace N. Axotomy-like changes of cat motoneuron electrical properties elicted y botulinum toxin depend on complete elimination of neuromuscular transmission. J Neurosci. 1991; 11:657–666. [PubMed: 1848281]

Pun S, Santos AF, Saxena S, Xu L, Caroni P. Selective vulnerability and pruning of phasic motoneuron axons in motoneuron disease alleviated by CNTF. Nat Neurosci. 2006; 9:408–419. [PubMed: 16474388]

Reddy LV, Koirala S, Sugiura Y, Herrera AA, Ko CP. Glial cells maintain synaptic structure and function and promote development of the neuromuscular junction in vivo. Neuron. 2003; 40:563–580. [PubMed: 14642280]

Reid R, Slater CR, Bewick GS. Synaptic Vesicle Dynamics in Rat Fast and Slow Motor Nerve Terminals. J Neuroscience. 1999; 19:2511–2521. [PubMed: 10087065]

Reynolds ML, Woolf CJ. Terminal Schwann cells elaborate extensive processes following denervation of the motor endplate. J Neurocytol. 1992; 21:50–66. [PubMed: 1346630]

Rochon D, Rousse I, Robitaille R. Synapse-glia interactions at the mammalian neuromuscular junction. J Neurosci. 2001; 21:3819–3829. [PubMed: 11356870]

Sagot Y, Dubois-Dauphin M, Tan SA, de Bilbao F, Aebischer P, Martinou J-C, Kato AC. Bcl-2 Overexpression Prevents Motoneuron Cell Body Loss but Not Axonal Degeneration in a Mouse Model of a Neurodegenerative Disease. J Neuroscience. 1995; 15:7727–7733. [PubMed: 7472523]

Sanes JR, Lichtman JW. Development of the Vertebrate Neuromuscular Junction. Annual Review of Neuroscience. 1999; 22:389–442.

Sanes JR, Lichtman JW. Induction, assembly, maturation and maintenance of a postsynaptic apparatus. Nat Rev Neurosci. 2001; 2:791–805. [PubMed: 11715056]

Schaefer AM, Sanes JR, Lichtman JW. A compensatory subpopulation of motor neurons in a mouse model of amyotrophic lateral sclerosis. J Comp Neurol. 2005; 490:209–219. [PubMed: 16082680]

Son YJ, Trachtenberg JT, Thompson WJ. Schwann cells induce and guide sprouting and reinnervation of neuromuscular junctions. Trends Neurosci. 1996; 19:280–285. [PubMed: 8799973]

Sugiura, Y.; Reddy, LV.; Yang, JF.; Ko, CP. The involvement of skeletal muscles in neurodegeneration in SOD1 mice. Washington D.C: Society for Neuroscience; 2004. Program No. 340.5

Todd KJ, Darabid H, Robitaille R. Perisynaptic glia discriminate patterns of motor nerve activity and influence plasticity at the neuromuscular junction. J Neurosci. 2010; 30:11870–11882. [PubMed: 20810906]

Turner BJ, Ackerley S, Davies KE, Talbot K. Dismutase-competent SOD1 mutant accumulation in myelinating Schwann cells is not detrimental to normal or transgenic ALS model mice. Hum Mol Genet. 2010; 19:815–824. [PubMed: 20008901]

Vabnick I, Shrager P. Ion channel redistribution and function during development of the myelinated axon. J Neurobiol. 1998; 37:80–96. [PubMed: 9777734]

Vabnick I, Messing A, Chiu SY, Levinson SR, Schachner M, Roder J, Li C, Novakovic S, Shrager P. Sodium channel distribution in axons of hypomyelinated and MAG null mutant mice. J Neurosci Res. 1997; 50:321–336. [PubMed: 9373041]

Wang L, Pytel P, Feltri ML, Wrabetz L, Roos RP. Selective knockdown of mutant SOD1 in Schwann cells ameliorates disease in G85R mutant SOD1 transgenic mice. Neurobiol Dis. 2012

Wong M, Martin LJ. Skeletal muscle-restricted expression of human SOD1 causes motor neuron degeneration in transgenic mice. Hum Mol Genet. 2010; 19:2284–2302. [PubMed: 20223753]

Wooley CM, Sher RB, Kale A, Frankel WN, Cox GA, Seburn KL. Gait analysis detects early changes in transgenic SOD1(G93A) mice. Muscle Nerve. 2005; 32:43–50. [PubMed: 15880561]

Highlights

- Terminal Schwann cells (TSCs) were studied in fast and slow muscles of $SOD1^{G93A}$ mice
- All P30 neuromuscular junctions (NMJs) were innervated but half in fast-type muscle lacked TSC cell bodies
- Almost all (95%) P30 NMJs in slow muscle possessed at least one TSC
- By P60, fast muscle showed 25% denervation whereas slow muscle showed 1% denervation
- TSC NMJ coverage at P30 is thus correlated with the extent of denervation found at P60

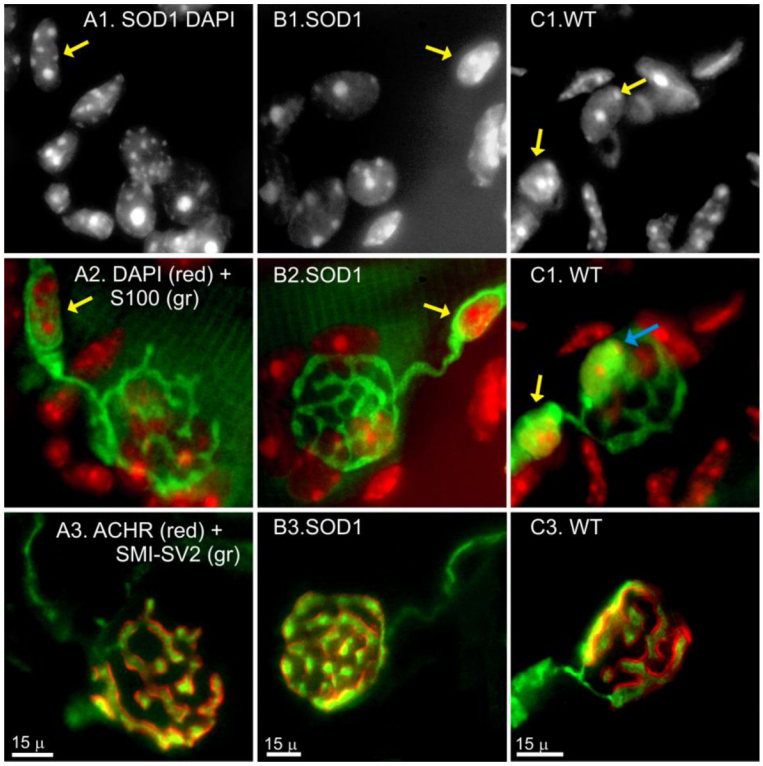

Figure 1.

Many P30 SOD1 MG NMJs lack TSCs. TSC and SC cell bodies were identified by DAPI and S100 colabeling. A1–2. Panel shows an MG NMJ labeled for DAPI only (A1) and merged with S100 labeling (green, DAPI shown in red, A2). In each panel, the yellow arrow indicates location of DAPI-S100 colabeling. Other DAPI-labeled nuclei visible in A1–2 belong to the underlying muscle fiber or to other, non-S100-expressing cells in the immediate vicinity. A3. Same endplate labeled for SMI-SV2 (green) and ACHRs (red), demonstrating that the endplate is fully innervated. In this example, no TSC cell bodies identified by DAPI-S100 colabeling can be seen at the endplate which is instead covered by the S100-labeled processes of an SC with a cell body located outside the endplate along the preterminal axon. B1–3. Labeling as in A. Panel B illustrates a second example of a P30 SOD1 MG NMJ in which the S100-labeled processes of a remotely-located SC cover the motor terminal of a fully innervated NMJ. These examples also illustrate the general finding that all P30 B6.SOD1 NMJs were supplied by a single motor axon. C1–3. Labeling as in A. Panels demonstrate labeling at a P30 WT MG NMJ. At this NMJ, a single TSC cell body (blue arrow, C2) is located at a fully-innervated endplate (C3). All P30 WT MG NMJs showed one or more endplate TSC cell body.

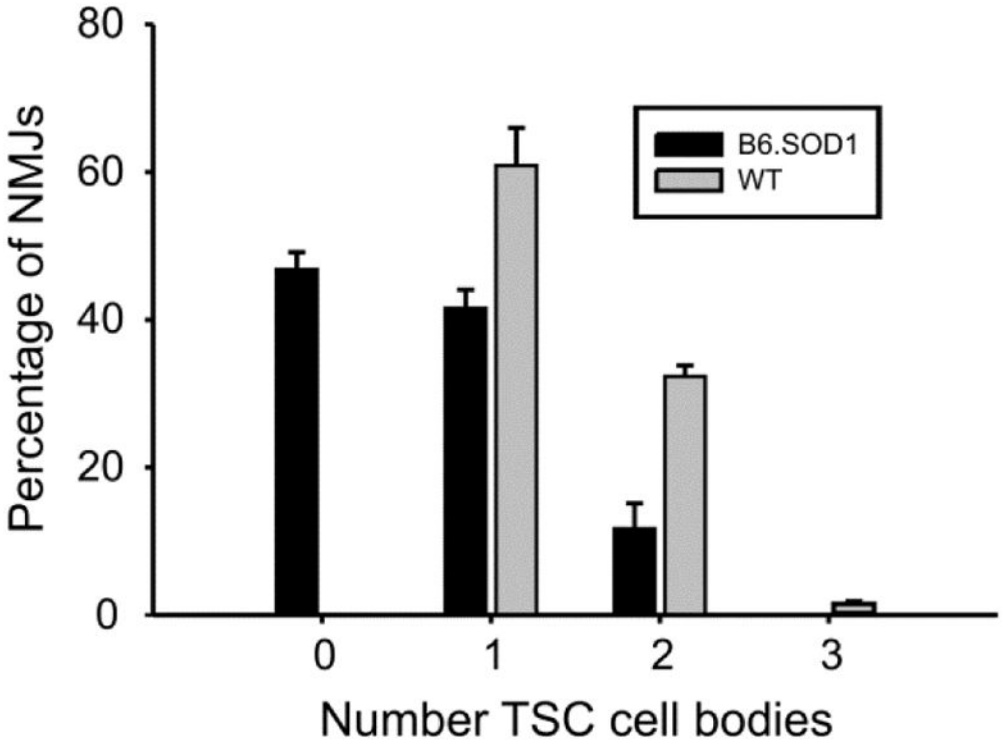

Figure 2.

Summary of P30 WT and B6.SOD1 MG TSC cell body counts. The number of TSC cell bodies located at NMJs and identified by DAPI-S100 colabeling were counted at WT and B6.SOD1 MG NMJs (N = 4 muscles in each group, 80 NMJs sampled in each muscle). Bars show mean values + 1 SEM. All NMJs in this analysis were fully-innervated as judged by SMI-SV2 labeling and fully-covered by S100 labeling as illustrated in Fig 1. An average of almost 50% of P30 B6.SOD1 MG NMJs lacked TSC cell bodies whereas all P30 WT MG NMJs had one of more TSC cell body located at NMJs. A nested ANOVA showed that the overall group means differed significantly ($p < 0.01$).

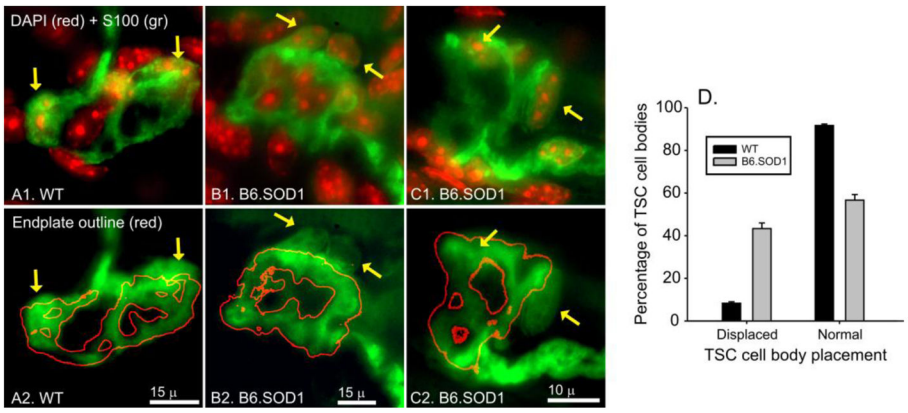

Figure 3.

Placement of WT and B6.SOD1 MG TSC cell bodies. Top row shows NMJs colabeled for DAPI and S100. Bottom row as described below. A1–2. Panel A1 illustrates a P30 WT MG NMJ which features 2 TSC cell bodies indicated by yellow arrows. A2. Muscle sections were also labeled for ACHRs. Images of ACHR labeling obtained in the same focal plane as A1 were processed using edge detection tools (ImageJ) to yield images of the outlines of ACHR labeling. These were then merged with S100 labeling images to produce the type of image shown in A2. This enabled assessment of the placement of identified TSC cell bodies relative to the outline of ACHR labeling. The image shown in A2 illustrates the 2 broad categories of TSC cell body placement. The left yellow arrow indicates a TSC cell body that is almost completely contained within the limits of ACHR labeling. This type of placement was categorized as being normal. The right yellow arrow indicates the second TSC whose cell body appeared to lie mostly outside the limits of ACHR labeling. This type of placement was categorized as being displaced. B1–2. Images were obtained from a P30 B6.SOD1 MG endplate. In this case, 2 TSC cells bodies were identified (B1) both of which appeared to lie immediately outside the limits of ACHR labeling (B2) and were thus categorized as being displaced. C1–2. Images were obtained from a second P30 B6.SOD1 MG endplate from the same muscle. 2 TSC cell bodies were identified (C1). The left TSC cell body was positioned normally while the right was displaced. D. Summary of TSC cell body placement data for P30 WT and B6.SOD1 MG NMJs. Bars show mean percentages of placement categories + 1 SEM (N = 4 muscles in each group, 80 NMJs sampled in each muscle). The majority (mean, 92%) of WT MG NMJs had normally-placed TSC cell bodies whereas B6.SOD1 NMJs featured a large fraction (45%) of displaced TSC cell bodies. Two-way table analysis showed that these distributions differed significantly (Pearson chi-square, $p < 0.01$).

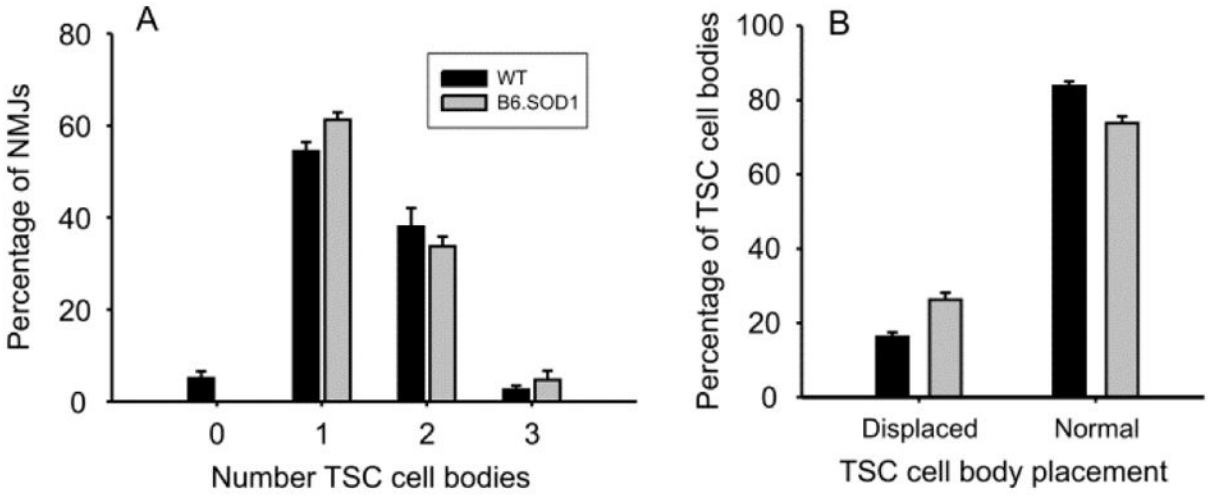

Figure 4.

P30 soleus TSC cell body number and placement. A. Bars show the distributions of mean TSC cell counts (+ 1 SEM) at P30 WT and B6.SOD1 soleus NMJs. For each group, N = 4 muscles, 80 NMJs sampled per muscle. Means values of TSC cell counts did not differ significantly between WT and B6.SOD1 soleus NMJs (nested ANOVA, $p > 0.05$). B. Distributions of mean (+ 1 SEM) TSC cell body placement percentages at NMJs for P30 WT and B6.SOD1 soleus NMJs. These distributions did not differ significantly (Pearson chi square, $p > 0.05$).

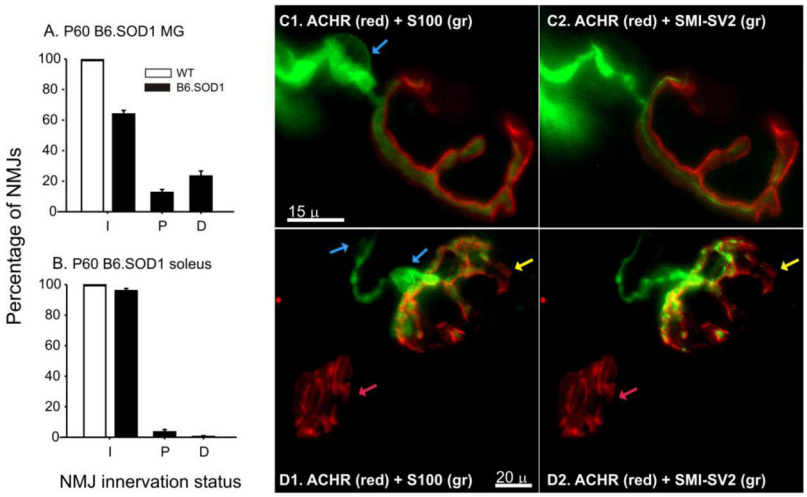

Figure 5.

P60 B6.SOD1 NMJ innervation and S100 coverage. NMJ innervation was assessed using SMI+SV2 and ACHR labeling and classified into 3 categories (I, fully-innervated; P, partially-innervated; D, denervated). Bar charts show the distributions of mean innervation percentages (+ 1 SEM) for P60 B6.SOD1 MG (A, N = 10 muscles) and soleus (B, N = 4 muscles). All P60 WT NMJs were fully innervated. The P60 B6.SOD1 MG distribution differed significantly from P60 WT and from P30 B6.SOD1 MG innervation distributions (Pearson chi square, $p < 0.01$). C1–2. Example of a P60 B6.SOD1 MG NMJ both fully-covered by S100 labeling (C1) and fully-innervated (C2). The blue arrow indicates the nucleus of an SC providing S100+ processes which cover this NMJ. D1–2. Upper NMJ. Example of a partially-innervated B6.SOD1 MG NMJ (D2, yellow arrow) which lacked S100 labeling where innervation labeling was absent (D1). Blue arrows indicate locations of SC nuclei determined by DAPI-S100 colabeling (not shown). In the same focal plane, a completely denervated NMJ is shown (lower left NMJ, red arrow, D2) which also completely lacked evidence of S100 labeling both over the endplate and in preterminal areas. S100 labeling at B6.SOD1 NMJs was classified into fully- and partially-covered and absent categories and cross-tabulated with innervation status categories. Analysis showed that innervation and S100 labeling categories corresponded such that the innervation status distributions shown in panels A, B also reflect S100 coverage categories where I (innervated) = fully covered by S100 labeling, P (partially innervated) = partially covered and D (denervated) = S100 coverage absent.

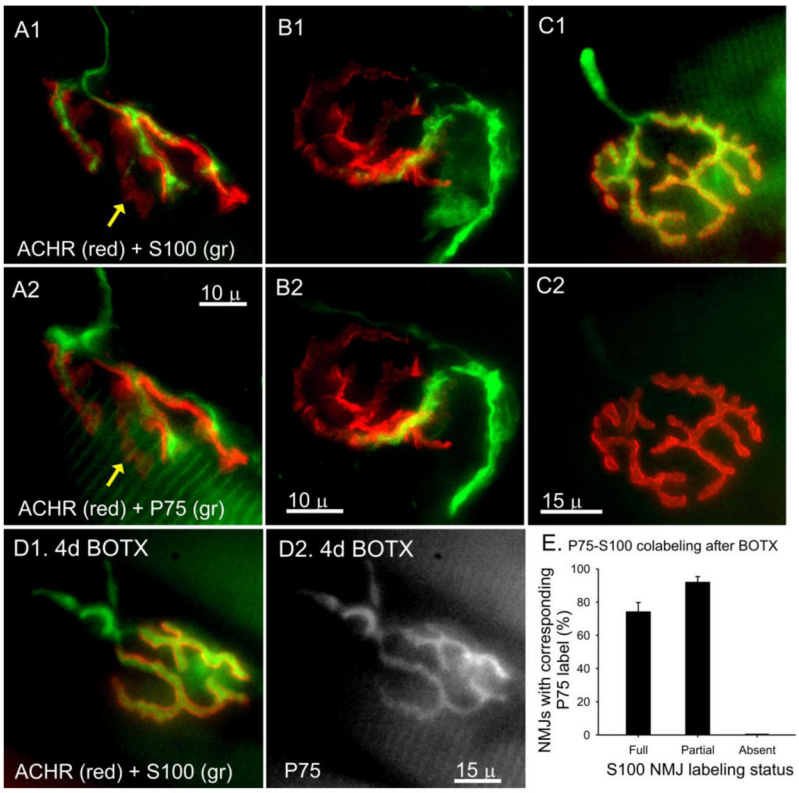

Figure 6.

P60 B6.SOD1 MG NMJ S100 and P75 colabeling patterns. Top row shows NMJs labeled for ACHRs (red) and S100 (green). Second row shows the same NMJs labeled for ACHRs (red) and P75 (green). A1–2. Example of an NMJ partially innervated (SMI-SV2 labeling not shown) and partially covered by S100 labeling (A1, label absent at yellow arrow) which is also colabeled for P75 (A2). B1–2. A second example of S100-P75 colabeling at a partially innervated and partially S100-covered B6.SOD1 MG NMJ. C1–2. Example of a fully innervated (SMI-SV2 labeling not shown) and fully S100-covered B6.SOD1 MG NMJ. In this case, no P75 labeling could be detected (C2). D1–2. Example of a fully-innervated (SMI-SV2 labeling not shown) and fully S100-covered B6.SOD1 MG NMJ 4d after intramuscular injection of botulinum toxin (BOTX). Overall, 4d BOTX paralysis did not affect innervation status or S100 coverage of B6.SOD1 MG NMJs. However, P75 expression appeared in all innervated and partially innervated MG NMJs. An example of such labeling for the NMJ in D1 is shown in D2. E. Summary of relationship between S100 and P75 labeling 4d after intramuscular injection of BOTX. The chart shows that an average of 0% of B6.SOD1 MG NMJs (N = 3 muscles) which lacked S100 labeling showed P75 labeling. By contrast, ca 91% and 76% of NMJs that showed partial or full S100 labeling, respectively, also showed P75 labeling 4d after intramuscular injection of BOTX.

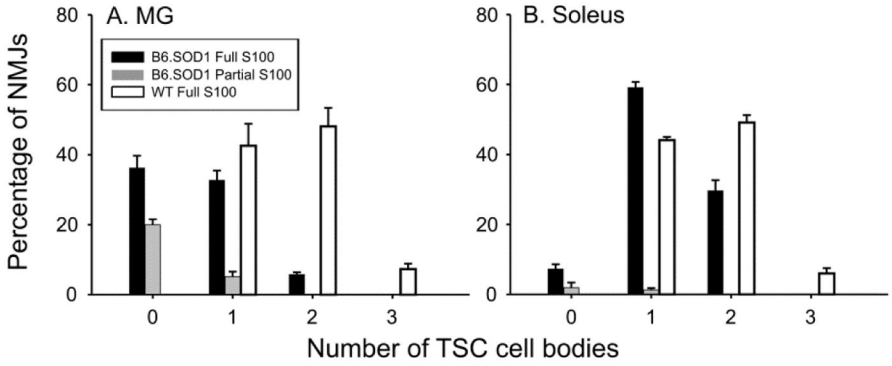

Figure 7.

Summary of TSC numbers at NMJs of P60 MG and soleus NMJs. A. MG muscles (N = 4, WT and B6.SOD1). Whereas no NMJs with partial S100 coverage were found at P30, at P60, a sizable fraction (20%) of B6.SOD1 MG NMJs possessed no TSC cell bodies and partial S100 coverage while about 37% lacked TSC cell bodies but showed full S100 coverage. As at P30, all P60 WT MG NMJs possessed one or more TSC cell body. In WT MG, average TSC cell count increased between P30 and P60 (P30, 1.36 ± 0.03; P60, 1.49 ± 0.03) but the increase was not significant ($p > 0.05$, nested ANOVA). B. Soleus muscles. Unlike P30, the mean number of TSC cell bodies at B6.SOD1 soleus NMJs was significantly less that WT ($p < 0.01$, nested ANOVA). Part of this difference is likely related to a small increase in WT soleus mean TSC number (P30, 1.43 ± 0.03; P60, 1.52 ± 0.03) which was not significant ($p > 0.05$, nested ANOVA). In addition, the mean number of TSC cell bodies at P60 B6.SOD1 soleus NMJs was less than the mean at P30 ($p < 0.01$, nested ANOVA). These data suggest that B6.SOD1 soleus NMJs may lose TSC cell bodies between P30 and P60.

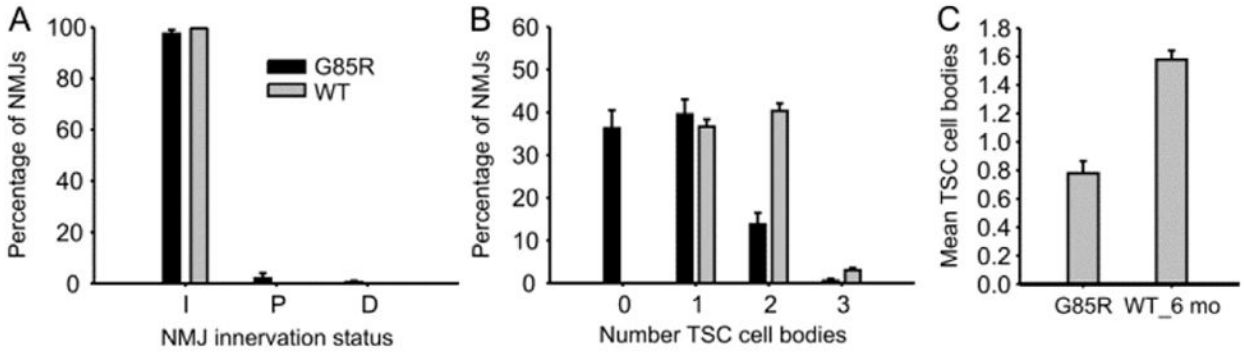

Figure 8.

Average TSC cell body number at 160d G85R MG NMJs is decreased. A. Data from 160d G85R MG NMJ was compared with data from 6 mo WT MG NMJs. No significant differences were found for innervation status or for S100 coverage (not shown). As found in P60 B6.SOD1 MG NMJs (Fig 5), S100 coverage mirrored NMJ innervation status. B. Chart demonstrates that the distribution of TSC number at G85R MG NMJs is shifted leftwards relative to 6 mo WT MG data and possesses a considerable percentage (37%) that lack TSC cell bodies. C. The mean number of TSC cell bodies at G85R MG NMJs was significantly less than 6 mo WT MG NMJs ($p < 0.01$, nested ANOVA).